


ARTICLE

Open Access

Emergence of the topological Hall effect in a tetragonal compensated ferrimagnet $\text{Mn}_{2.3}\text{Pd}_{0.7}\text{Ga}$

Won-Young Choi¹, Woosuk Yoo¹ and Myung-Hwa Jung¹ 

Abstract

Topological spin textures such as magnetic skyrmions have attracted considerable interest due to their potential application in spintronic devices. However, there still remain several challenges to overcome before their practical application, for instance, achieving high scalability and thermal stability. Recent experiments have proposed a new class of skyrmion materials in the Heusler family, $\text{Mn}_{1.4}\text{Pt}_{0.9}\text{Pd}_{0.1}\text{Sn}$ and $\text{Mn}_2\text{Rh}_{0.95}\text{Ir}_{0.05}\text{Sn}$, which possess noncollinear magnetic structures. Motivated by these experimental results, we suggest another Heusler compound hosted by Mn_3Ga to overcome the above limitations. We fabricate $\text{Mn}_{3-x}\text{Pd}_x\text{Ga}$ thin films, focusing on the magnetic compensation point. In $\text{Mn}_{2.3}\text{Pd}_{0.7}\text{Ga}$, we find a spin-reorientation transition around $T_{\text{SR}} = 320$ K. Below the T_{SR} , we observe the topological Hall effect and a positive magnetic entropy change, which are the hallmarks of a chiral noncollinear spin texture. By integrating all the data, we determine the magnetic phase diagram, displaying a wide chiral noncollinear spin phase even at room temperature. We believe that this compensated ferrimagnet shows promise for opening a new avenue toward chiral spin-based, high-density, and low-power devices.

Introduction


Topologically protected spin phases, such as magnetic skyrmions, show promise for future applications in non-volatile memory and spintronic devices after being initially observed in MnSi bulk material^{1–4}. To date, various mechanisms for generating this intriguing magnetic phase have been theoretically and experimentally identified, such as long-range magnetic dipolar interactions competing with perpendicular magnetic anisotropy^{5–7}, Dzyaloshinskii-Moriya (DM) interactions², the interplay of Ruderman-Kittel-Kasuya-Yosida (RKKY) and four-spin exchange interactions⁸, and geometrically frustrated spin systems⁹. These mechanisms operate separately or in tandem to generate skyrmion phases in many chiral magnets. An unconventional spin texture with scalar spin chirality acts as an effective magnetic field, resulting in the topological Hall effect (THE)^{10,11}. Thus, the THE is often interpreted as a signature of a chiral spin texture, such as a magnetic skyrmion. Recently, in Mn-based tetragonal

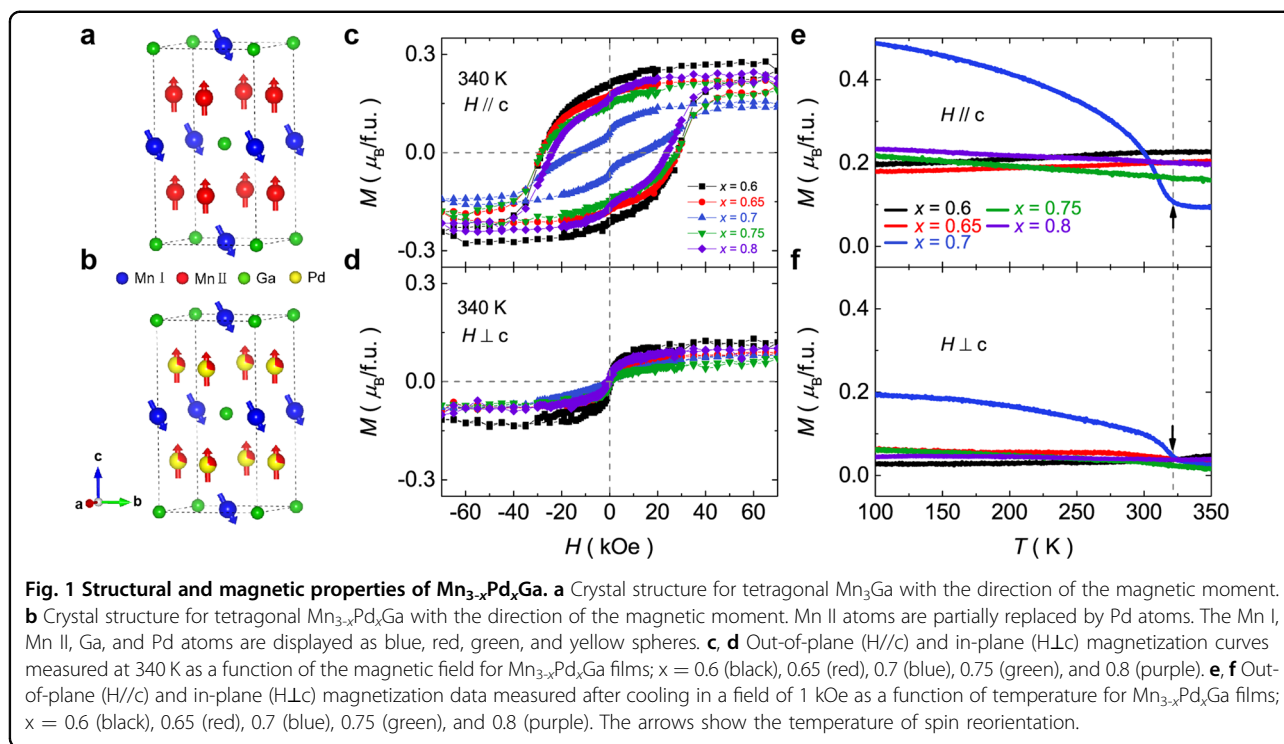
Heusler compounds such as $\text{Mn}_{1.4}\text{Pt}_{0.9}\text{Pd}_{0.1}\text{Sn}$ ^{12,13} and $\text{Mn}_2\text{Rh}_{0.95}\text{Ir}_{0.05}\text{Sn}$ ¹⁴, it has been reported that the other spin chirality of the antiskyrmion lattice is stabilized via strong spin-orbit coupling and structural symmetry breaking by Pd and Ir doping. However, despite the observation of a chiral spin texture in a variety of materials, there are some issues that must be overcome before their practical application. First, the spin chirality needs to be stabilized at room temperature so that it is not disturbed by thermal fluctuations¹⁵. Second, a low saturation magnetization is required to produce a small stray field for high-density devices¹⁴. For the above examples, the antiskyrmion state in $\text{Mn}_2\text{Rh}_{0.95}\text{Ir}_{0.05}\text{Sn}$ is stable up to 400 K, but the total magnetic moment is considerably high ($\sim 4 \mu_{\text{B}}/\text{f.u.}$)¹². On the other hand, the magnetization value of $\text{Mn}_2\text{Rh}_{0.95}\text{Ir}_{0.05}\text{Sn}$ is relatively low ($\sim 1 \mu_{\text{B}}/\text{f.u.}$), but the antiskyrmion state emerges at lower temperatures up to ~ 250 K¹⁴. As a potential candidate for designing stable skyrmions at room temperature together with a low saturation magnetization to overcome the aforementioned issues, we focus on a Mn_3Ga host Heusler compound. More detailed comparisons with other materials

Correspondence: Myung-Hwa Jung (mhjung@sogang.ac.kr)

¹Department of Physics, Sogang University, Seoul 04107, Republic of Korea

© The Author(s) 2021, corrected publication 2022

 **Open Access** This article is licensed under a Creative Commons Attribution 4.0 International License, which permits use, sharing, adaptation, distribution and reproduction in any medium or format, as long as you give appropriate credit to the original author(s) and the source, provide a link to the Creative Commons license, and indicate if changes were made. The images or other third party material in this article are included in the article's Creative Commons license, unless indicated otherwise in a credit line to the material. If material is not included in the article's Creative Commons license and your intended use is not permitted by statutory regulation or exceeds the permitted use, you will need to obtain permission directly from the copyright holder. To view a copy of this license, visit <http://creativecommons.org/licenses/by/4.0/>.



hosting chiral spin textures are listed in Table S1 of the Supplementary Information.

The undoped compound Mn_3Ga is ferrimagnetic with a Curie temperature of $T_C = 820$ K and crystallizes in a D_{022} tetragonal structure with perpendicular magnetic anisotropy (PMA)¹⁶. Two inequivalent Mn sublattices, Mn I and Mn II, possess different magnetic moments of $3.1 \mu_B/\text{f.u.}$ and $4.2 \mu_B/\text{f.u.}$, which are coupled antiferromagnetically and lead to a total magnetization of $\sim 1.1 \mu_B/\text{f.u.}$ ¹⁷. Interestingly, a recent neutron scattering experiment revealed that tetragonal Mn_3Ga has an in-plane tilted spin structure (Fig. 1a)¹⁷, where the magnetic moment at the Mn II site is fixed along the c -axis and the direction of the magnetic moment at the Mn I site is tilted in the ab plane, leading to an in-plane magnetic component at low magnetic fields. Additionally, there is oscillatory exchange coupling from the first and second nearest neighbors depending on the distance between the Mn sublattices¹⁷. Moreover, previous studies reported that the magnetic properties of Mn_3Ga can be tuned by substituting a transition metal for Mn II in $\text{Mn}_{3-x}\text{Y}_x\text{Ga}$, such as $\text{Y} = \text{Pt}, \text{Pd}, \text{Co},$ and Ni , and can be fully compensated with a zero net magnetic moment¹⁸. A typical example of magnetic compensation is when $\text{Y} = \text{Pt}$ ^{18,19}. The net magnetization changes from ferrimagnetic to completely compensated at $x = 0.65$ in $\text{Mn}_{3-x}\text{Pt}_x\text{Ga}$, demonstrating a fully compensated ferrimagnetic state. However, there has been no report on the THE being observed at the magnetic compensation point in Mn_{3-}

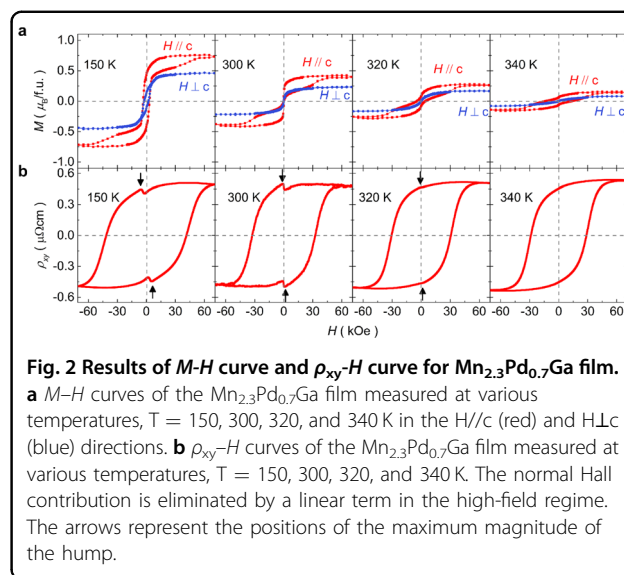
$x\text{Pt}_x\text{Ga}$, where the noncollinear spin texture is maximally expected¹⁹. This is compared to $\text{Mn}_{1.4}\text{Pt}_{0.9}\text{Pd}_{0.1}\text{Sn}$, in which they reported a spin-reorientation transition from a collinear ferromagnetic to a noncollinear configuration below $T_{\text{SR}} = 135$ K, accompanied by the topological Hall effect but with no magnetic compensation²⁰. Among the magnetic interactions mentioned above, the role of DM interactions is essential to lead to scalar spin chirality. The crucial elements of DM interactions are strong spin-orbit coupling and structural symmetry breaking²¹. Thus, we deduce the possibility of forming scalar spin chirality through heavy metal substitution in Mn_3Ga . Heavy metals can act as crucial elements of DM interactions for strong spin-orbit coupling and structural symmetry breaking. Recently, the observation of positive magnetic entropy was proposed to be additional evidence of skyrmion formation²². The magnetic entropy change is interpreted as a transition from magnetic order to disorder states. For example, when a system in an external field transits from an ordered spin state such as a fully saturated ferromagnetic phase (low entropy) to a highly disordered spin state such as a skyrmion phase (high entropy), the change in magnetic entropy becomes positive²². The magnetic entropy change can be measured using isothermal magnetization with a constant temperature interval^{22,23}.

In our study, we chose the $4d$ element Pd as the substitution atom because, compared to the $5d$ element Pt, Pd is well magnetized and is expected to contribute to the complex spin configuration (Fig. 1b)²⁴. We fabricated

$\text{Mn}_{3-x}\text{Pd}_x\text{Ga}$ ($x = 0.6, 0.65, 0.7, 0.75,$ and 0.8) thin films (see Supplementary Figs. S1 and S2). The compensation point, theoretically reported as $x \sim 0.65$ ¹⁸, was experimentally confirmed by the minimized magnetization ($=0.14 \mu_B/\text{f.u.}$) at 340 K. In addition to the ferromagnetic behavior well above room temperature, $\text{Mn}_{2.3}\text{Pd}_{0.7}\text{Ga}$ exhibited a transition to a state with a higher magnetic moment below $T_{\text{SR}} = 320$ K, which was assigned to a spin-reorientation transition. The low magnetic moment at the compensation point could be accounted for by considering a noncollinear spin alignment. In the $\text{Mn}_{2.3}\text{Pd}_{0.7}\text{Ga}$ thin film, we observed a considerable topological Hall effect and positive magnetic entropy change at temperatures up to 320 K, which was the spin-reorientation transition of $\text{Mn}_{2.3}\text{Pd}_{0.7}\text{Ga}$. We also determined the magnetic phase diagram from the topological Hall effect and magnetic entropy data, suggesting that a chiral noncollinear spin structure such as skyrmions was present in the tetragonal compensated ferrimagnet $\text{Mn}_{2.3}\text{Pd}_{0.7}\text{Ga}$. This Heusler-based compensated ferrimagnet is a potential candidate for use in high-density and low-power data storage memory devices by replacing conventional magnetic materials.

Results and discussion

A series of $\text{Mn}_{3-x}\text{Pd}_x\text{Ga}$ ($x = 0.6, 0.65, 0.7, 0.75,$ and 0.8) thin films were prepared on a clean MgO substrate to investigate the magnetic compensation point. Figure 1c, d show the magnetic field dependence of magnetization and $M-H$ curves measured at 340 K. The magnetic fields were applied perpendicular ($H//c$) and parallel ($H\perp c$) to the film plane. Regarding $H//c$, the $\text{Mn}_{3-x}\text{Pd}_x\text{Ga}$ films exhibit clear hysteresis loops, indicating that the ferrimagnetic state persists well above room temperature with perpendicular magnetic anisotropy even after Pd substitution. The coercive fields are approximately $H_C = 30$ kOe, except $H_C = 15$ kOe for $x = 0.7$. With increasing Pd concentration, the saturation magnetization decreases and becomes the minimum ($M_S = 0.14 \mu_B/\text{f.u.}$) at $x = 0.7$. This result demonstrates the compensated ferrimagnetic state of $\text{Mn}_{2.3}\text{Pd}_{0.7}\text{Ga}$, which is consistent with the theoretical report¹⁸. Here, there are discontinuous steps around the zero field in the $M-H$ curves, which can be attributed to the existence of secondary magnetic phases such as D0_{19} hexagonal Mn_3Ga , L2_1 cubic Mn_3Ga , or D0_{22} tetragonal Mn_2Ga . However, in the Supplementary Information, we describe the reasons why the coexistence of two magnetic phases can be ruled out. On the other hand, regarding $H\perp c$, there exists an in-plane magnetic component caused by the canted Mn I moment, as previously mentioned in Fig. 1a, b. For further study on the magnetic properties that depend on the Pd concentration, we measured the temperature dependence of the



magnetization $M-T$ curves. The data were taken after cooling in a 1 kOe field for the $H//c$ and $H\perp c$ configurations. As shown in Fig. 1e, f, only the $x = 0.7$ sample undergoes a transition to a state with a higher magnetic moment at $T_{\text{SR}} = 320$ K, while the other samples show nearly temperature-independent behavior. We assign the magnetic ordering at T_{SR} to a spin reorientation transition, which is an additional magnetic state probably caused by the chiral noncollinear spin texture in the compensated ferrimagnet of $\text{Mn}_{2.3}\text{Pd}_{0.7}\text{Ga}$.

To unveil the origin of the spin reorientation transition of the compensated ferrimagnet $\text{Mn}_{2.3}\text{Pd}_{0.7}\text{Ga}$, we carried out detailed magnetic and electrical measurements at various temperatures above and below the T_{SR} . The comparison of $\text{Mn}_{3-x}\text{Pd}_x\text{Ga}$ films with different x values is displayed in Fig. S3 in the Supplementary Information. Remarkably, unusual magnetic properties are observed only in the compensated ferrimagnet when $x = 0.7$. In Fig. 2a, we depict the $M-H$ curve results of $x = 0.7$ measured at $T = 150$ K, 300 K, 320 K, and 340 K in both the $H//c$ and $H\perp c$ configurations. The M_S values at all temperatures are lower than those reported in undoped Mn_3Ga ¹⁷. It is apparent that $\text{Mn}_{2.3}\text{Pd}_{0.7}\text{Ga}$ exhibits dramatic changes in the $M-H$ curves at $T < T_{\text{SR}}$, while being ferrimagnetic with perpendicular anisotropy. As the temperature decreases, the M_S values of $H//c$ and $H\perp c$ increase to approximately $0.75 \mu_B/\text{f.u.}$ and $0.5 \mu_B/\text{f.u.}$, respectively. The H_C value of $H//c$ gradually decreases with decreasing temperature and becomes nearly zero at room temperature; then, it increases again to $H_C \sim 3.5$ kOe at 150 K. The most striking feature is that at 300 K, H_C approaches zero, but the hysteresis loop is maintained in the high-field regime. This unconventional form of the magnetic hysteresis loop just below the T_{SR} is not an $M-H$ curve commonly observed in a ferromagnet or ferrimagnet.

Furthermore, an apparent hysteresis loop of $H \perp c$, which is not expected in the undoped Mn_3Ga tetragonal ferrimagnet phase, is observed at 150 K. These results imply that the spin configuration of the compensated ferrimagnet, $\text{Mn}_{2.3}\text{Pd}_{0.7}\text{Ga}$, is not a typical form below T_{SR} , thus changing the magnetic anisotropy. As reported earlier¹⁷, the tetragonal ferrimagnet of Mn_3Ga has an oscillatory exchange interaction depending on the distance between Mn moments along with the uniaxial anisotropy energy; thus, the strength of exchange coupling at each Mn site can be tuned by changing the lattice parameter. In this study, we observed a lattice expansion of $c = 7.15 \text{ \AA}$ for the c -axis parameter of $\text{Mn}_{2.3}\text{Pd}_{0.7}\text{Ga}$ from the reported value of $c \sim 7.11 \text{ \AA}$ of Mn_3Ga ¹⁶, which can cause a more canted Mn I moment. Therefore, the in-plane magnetization component enhanced by Pd substitution can be interpreted as being due to the weakened anti-ferromagnetic interaction between Mn moments. Furthermore, a careful look at the $M-H$ curve of $\text{Mn}_{2.3}\text{Pd}_{0.7}\text{Ga}$ provides the possible existence of DM interactions, which were theoretically proposed¹⁸. The DM interactions can be supported by inversion symmetry breaking and strong spin-orbit coupling due to the substitution of the $4d$ element Pd. In this regard, $\text{Mn}_{2.3}\text{Pd}_{0.7}\text{Ga}$ is a candidate to realize the DM interactions that lead to the formation of a chiral noncollinear spin texture.

Figure 2b shows the Hall resistivity, ρ_{xy} , taken at the same temperatures as the magnetic measurements above. There is no temperature dependence of the normal Hall effect (see Supplementary Fig. S4), and we subtract the normal Hall contribution using the linear slope in the high-field regime. The ρ_{xy} data clearly show the anomalous Hall effect at all temperatures. It is clearly seen that the anomalous Hall resistivity values at $H = 70 \text{ kOe}$ are nearly temperature independent compared to the strong temperature dependence of M_S ; notably, this is different from what is commonly known. Regarding $\text{Mn}_{2.3}\text{Pd}_{0.7}\text{Ga}$, we observe a nonlinear relation between the magnetization and anomalous Hall resistivity (see Supplementary Fig. S5), which cannot be described by the ferromagnetic component alone and can be attributed to the noncollinear spin texture^{8,9,25}. Here, it is noteworthy that there is an unexpected hump-like anomaly in the low-magnetic-field regime of the ρ_{xy} data below 320 K, which is the spin-reorientation temperature, T_{SR} . In addition, note that this hump is only present in the $\text{Mn}_{2.3}\text{Pd}_{0.7}\text{Ga}$ sample (see Supplementary Fig. S6). The black arrow represents the position of the maximum value of the hump. At temperatures below the T_{SR} , a hump-like anomaly starts to appear and moves to higher fields as the temperature is decreased. The overall shape of the anomaly is similar to the topological Hall effect (THE) reported in various skyrmion materials^{10,26}.

Typically, a noncollinear spin state such as a magnetic skyrmion emerges in the low-field region immediately after which the aligned spins generate magnetic stripe domains around the zero field^{2,7,13}. Therefore, we predict that if the skyrmion state emerges, the magnetoresistance (MR) becomes a maximum at the stripe domain state due to the anisotropic magnetoresistance (AMR), which exhibits a low (high) resistance when the direction of magnetization is perpendicular (parallel) to the current direction²⁴. Thus, we measured the MR of $\text{Mn}_{2.3}\text{Pd}_{0.7}\text{Ga}$ at the same temperatures for comparison. In Fig. 3a, b, we plot the magnified data of $|\rho_{xy}|$ and MR in the low-field regime ranging from -10 kOe to 10 kOe . It is apparent that the position of the emerging point of the THE is well matched with the maximum position of MR, as predicted above. Moreover, we observe the signature of weak (anti) localization in both the longitudinal and perpendicular MR curves (see Supplementary Fig. S7), indicating the strong spin-orbit coupling required for the realization of DM interactions that give rise to the formation of skyrmions. This result also supports our hypothesis for the Pd substitution effect, which plays an important role in strong spin-orbit coupling and structural symmetry breaking.

Direct magnetic imaging is available using real-space measurements such as Lorentz transmission electron microscopy and magnetic force microscopy (MFM)^{2,13}. Therefore, we carried out MFM measurements by varying the temperature from one sample to another in many different positions. However, we could not observe any magnetic domain structure in the compensated ferrimagnet of $\text{Mn}_{2.3}\text{Pd}_{0.7}\text{Ga}$. This is because the stray field is locally canceled by antiparallel spins²⁷. An alternative approach to provide a hint for the possible presence of a

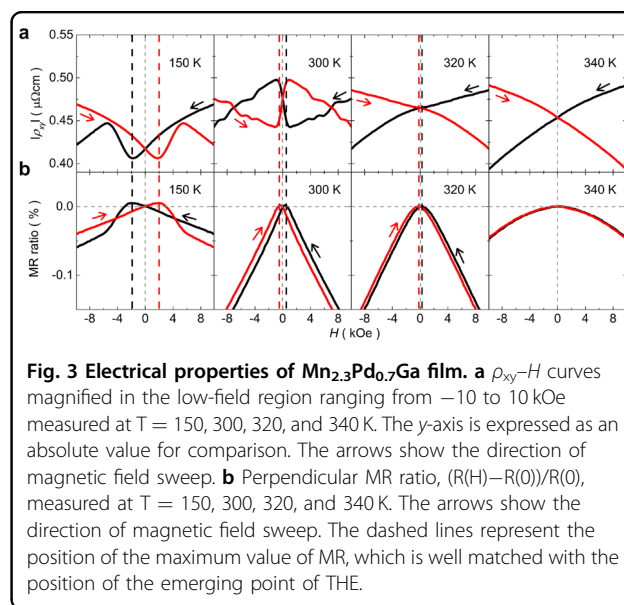


Fig. 3 Electrical properties of $\text{Mn}_{2.3}\text{Pd}_{0.7}\text{Ga}$ film. **a** $\rho_{xy}-H$ curves magnified in the low-field region ranging from -10 to 10 kOe measured at $T = 150, 300, 320,$ and 340 K . The y-axis is expressed as an absolute value for comparison. The arrows show the direction of magnetic field sweep. **b** Perpendicular MR ratio, $(R(H)-R(0))/R(0)$, measured at $T = 150, 300, 320,$ and 340 K . The arrows show the direction of magnetic field sweep. The dashed lines represent the position of the maximum value of MR, which is well matched with the position of the emerging point of THE.

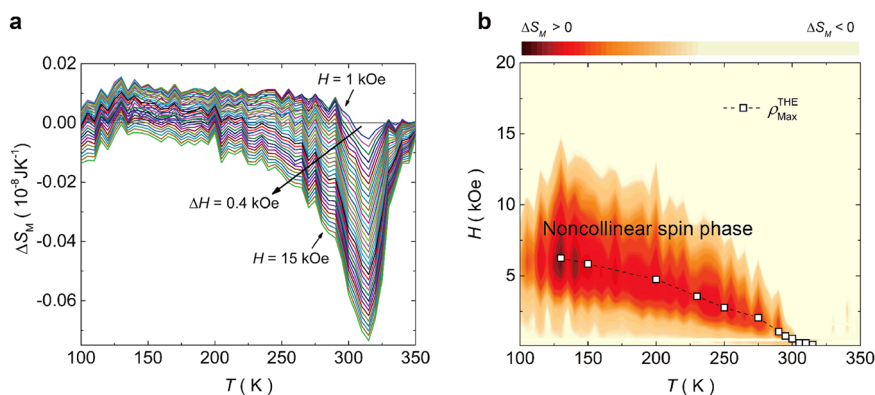


Fig. 4 Magnetic phase diagram for the $\text{Mn}_{2.3}\text{Pd}_{0.7}\text{Ga}$ film. **a** Temperature dependence of the magnetic entropy change, ΔS_M . The temperature interval is used as $\Delta T = 5$ K. Each line represents the different field range of integration, $\Delta H = 0.4$ kOe. The top line depicts the integrated field range, $H = 1$ kOe, and the bottom line depicts the integrated field range, $H = 15$ kOe. **b** H - T magnetic phase diagram derived from the positive ΔS_M (red-shaded area) and the maximum THE (open square symbols).

noncollinear spin state is the magnetic entropy change²². We calculated the magnetic entropy change, ΔS_M , by using the relation $\Delta S_M = \frac{1}{\Delta T} \left[\int_0^H (M_1) dH - \int_0^H (M_2) dH \right]$ from the isothermal magnetization curves for constant temperature intervals^{22,23}. Figure 4a shows the temperature dependence of ΔS_M . The temperature interval is $\Delta T = 5$ K, and each line represents the different field range of integration, $\Delta H = 0.4$ kOe. The ΔS_M data reveal positive values starting at room temperature. Using the broad scan of the magnetic entropy change ranging from 100 K to 350 K with the integrated external field ranging from 0.1 kOe to 20 kOe, we plot a contour map in Fig. 4b, where the x -axis is the temperature, the y -axis is the magnetic field, and the z -axis is the magnetic entropy change. Thus, we determined the H - T magnetic phase diagram of the $\text{Mn}_{2.3}\text{Pd}_{0.7}\text{Ga}$ film.

As we expected, a positive ΔS_M (red and black areas) starts to emerge at temperatures below the T_{SR} . The noncollinear spin phase expands as the temperature is decreased down to ~ 130 K, and then it begins to contract again. For the comparison of ΔS_M with the THE, we take the field values of the maximum magnitude of the hump from the ρ_{xy} - H plots in Fig. 2b, which are marked with open square symbols in Fig. 4b. Note that the pure topological Hall signals could not be directly extracted from the measured ρ_{xy} data. This is presumably due to complex exchange interactions caused by geometrically frustrated spins at the magnetic compensation point, as reported earlier in regard to GdRu_2Si_2 hosting noncollinear spin textures by four-spin exchange interactions⁸. In Fig. 4b, we plot the position of the maximum values of the THE, together with the area of the positive ΔS_M . It is remarkable that the two data points, namely, the THE maximum and the positive ΔS_M , considerably overlap. Furthermore, as the range of positive ΔS_M begins to

contract, the magnitude of the THE also starts to decrease and finally becomes zero at $T = 100$ K. From this figure, it is clear that the noncollinear spin phase is stable over a wide range of temperatures above room temperature. In addition, note that there is a high possibility of a skyrmion phase that occurs in the compensated ferrimagnet $\text{Mn}_{2.3}\text{Pd}_{0.7}\text{Ga}$ with relatively low magnetization.

Conclusion

In summary, we experimentally confirmed the magnetic compensation point of $\text{Mn}_{3-x}\text{Pd}_x\text{Ga}$ ($0.6 \leq x \leq 0.8$) to be $x = 0.7$. Tetragonal Mn_3Ga with a noncollinear spin configuration could be tuned by introducing the heavy metal element Pd for substitution, giving rise to structural symmetry breaking and strong spin-orbit coupling. We found a spin-reorientation transition at $T_{SR} = 320$ K, which is above room temperature. Below T_{SR} , we observed the topological Hall effect and a positive magnetic entropy change, originating from the chiral noncollinear spins of $\text{Mn}_{2.3}\text{Pd}_{0.7}\text{Ga}$. Currently, the application of chiral spin-based spintronics is a very important issue. Therefore, we hope that our findings of a compensated ferrimagnet phase emerging above room temperature with a quite low magnetization will open the possibility for new chiral spin devices.

Experimental method

$\text{Mn}_{3-x}\text{Pd}_x\text{Ga}$ ($0.6 \leq x \leq 0.8$) thin films with a thickness of 100 nm were deposited on a MgO (001) substrate by DC and RF magnetron sputtering systems at a base pressure on the order of 10^{-6} Torr. Using three targets, namely, Mn_2Ga , Mn, and Pd, the films were cosputtered at 400°C with an Ar pressure of 2 mTorr during deposition. We basically followed the detailed growth conditions for Mn_3Ga thin films reported elsewhere^{16,28}. To change the substitution rate of Pd for Mn, the working current of the

Pd target gun was varied from 16 mA to 20 mA while maintaining the other growth conditions. After deposition, a 2-nm-thick SiO₂ capping layer was deposited by in situ sputtering in the same chamber at room temperature to prevent oxidation. The chemical composition of Mn_{3-x}Pd_xGa was determined by energy dispersive X-ray (EDX) spectroscopy. The crystal structure was investigated using X-ray diffraction (XRD) with a Cu K α radiation source. The magnetic and electrical properties were measured with a superconducting quantum interference device-vibrating sample magnetometer (SQUID-VSM) in magnetic fields up to 70 kOe and at temperatures down to 2 K. The electrical measurements were carried out with the van der Pauw method. To avoid the possible discrepancy caused by shape anisotropy, the same films were used for all measurements.

Acknowledgements

This work was supported by the National Research Foundation of Korea (NRF) (grant no. 2020R1A2C3008044) and by Samsung Electronics Co., Ltd.

Author contributions

M.-H.J. conceived the original idea and wrote the paper with W.Y.C. Additionally, W.Y.C. and W.Y. designed the experiments and performed the measurements. Finally, W.Y.C. carried out the data analyses under the supervision of M.-H.J. All authors discussed the results and commented on the manuscript.

Conflict of interest

The authors declare no competing interests.

Publisher's note

Springer Nature remains neutral with regard to jurisdictional claims in published maps and institutional affiliations.

Supplementary information The online version contains supplementary material available at <https://doi.org/10.1038/s41427-021-00347-3>.

Received: 10 June 2021 Revised: 23 September 2021 Accepted: 28 September 2021

Published online: 24 December 2021

References

- Neubauer, A. et al. Topological hall effect in the a phase of MnSi. *Phys. Rev. Lett.* **102**, 1–4 (2009).
- Nagaosa, N. & Tokura, Y. Topological properties and dynamics of magnetic skyrmions. *Nat. Nanotechnol.* **8**, 899–911 (2013).
- Vedmedenko, E. Y. et al. The 2020 magnetism roadmap. *J. Phys. D Appl. Phys.* **53**, 453001 (2020).
- Back, C. H. et al. The 2020 skyrmionics roadmap. *J. Phys. D Appl. Phys.* **53**, 363001 (2020).
- Takao, S. A study of magnetization distribution of submicron bubbles in sputtered Ho-Co thin films. *J. Magn. Magn. Mater.* **31–34**, 1009–1010 (1983).
- Lin, Y. S., Grundy, P. J. & Giess, E. A. Bubble domains in magnetostatically coupled garnet films. *Appl. Phys. Lett.* **23**, 485–487 (1973).
- Kwon, H. Y., Bu, K. M., Wu, Y. Z. & Won, C. Effect of anisotropy and dipole interaction on long-range order magnetic structures generated by Dzyaloshinskii-Moriya interaction. *J. Magn. Magn. Mater.* **324**, 2171–2176 (2012).
- Khanh, N. D. et al. Nanometric square skyrmion lattice in a centrosymmetric tetragonal magnet. *Nat. Nanotechnol.* **15**, 444 (2020).
- Kurumaji, T. et al. Skyrmion lattice with a giant topological Hall effect in a frustrated triangular-lattice magnet. *Science* **365**, 914–918 (2019).
- Rout, P. K., Madduri, P. V. P., Manna, S. K. & Nayak, A. K. Field-induced topological Hall effect in the noncoplanar triangular antiferromagnetic geometry of Mn₃Sn. *Phys. Rev. B* **99**, 094430 (2019).
- Rana, K. G. et al. Observation of topological Hall effect in Mn₂RhSn films. *New J. Phys.* **18**, 085007 (2016).
- Nayak, A. K. et al. Magnetic antiskyrmions above room temperature in tetragonal Heusler materials. *Nature* **548**, 561–566 (2017).
- Ma, T. et al. Tunable magnetic antiskyrmion size and helical period from nanometers to micrometers in a D_{2d} heusler compound. *Adv. Mater.* **32**, 1–7 (2020).
- Jena, J. et al. Observation of magnetic antiskyrmions in the low magnetization ferromagnet Mn₂Rh_{0.95}Ir_{0.05}Sn. *Nano Lett.* **20**, 59–65 (2020).
- Leroux, M. et al. Skyrmion lattice topological hall effect near room temperature. *Sci. Rep.* **8**, 15510 (2018).
- Bang, H. et al. Structural, magnetic, and electrical properties of collinear antiferromagnetic heteroepitaxy cubic Mn₃Ga thin films. *Appl. Phys. Lett.* **115**, 012402 (2019).
- Rode, K. et al. Site-specific order and magnetism in tetragonal Mn₃Ga thin films. *Phys. Rev. B* **87**, 1–14 (2013).
- Sahoo, R. et al. Compensated ferrimagnetic tetragonal heusler thin films for antiferromagnetic spintronics. *Adv. Mater.* **28**, 8499–8504 (2016).
- Nayak, A. K. et al. Design of compensated ferrimagnetic Heusler alloys for giant tunable exchange bias. *Nat. Mater.* **14**, 679–684 (2015).
- Kumar, V. et al. Detection of antiskyrmions by topological Hall effect in Heusler compounds. *Phys. Rev. B* **101**, 14424 (2020).
- Moriya, T. Anisotropic superexchange interaction and weak ferromagnetism. *Phys. Rev.* **120**, 91–98 (1960).
- Jamaluddin, S. et al. Robust antiskyrmion phase in bulk tetragonal Mn–Pt (Pd)–Sn heusler system probed by magnetic entropy change and AC-susceptibility measurements. *Adv. Funct. Mater.* **29**, 2–7 (2019).
- Phan, M.-H. & Yu, S.-C. Review of the magnetocaloric effect in manganite materials. *J. Magn. Magn. Mater.* **308**, 325–340 (2007).
- Getzlaff, M. *Fundamentals of Magnetism*. (Springer Berlin Heidelberg, 2008).
- Li, Y. et al. Robust formation of skyrmions and topological hall effect anomaly in epitaxial thin films of MnSi. *Phys. Rev. Lett.* **110**, 1–5 (2013).
- Qin, Q. et al. Emergence of topological hall effect in a SrRuO₃ single layer. *Adv. Mater.* **31**, 1–6 (2019).
- Gao, S. et al. Fractional antiferromagnetic skyrmion lattice induced by anisotropic couplings. *Nature* **586**, 37–41 (2020).
- Bang, H. W. et al. Perpendicular magnetic anisotropy properties of tetragonal Mn₃Ga films under various deposition conditions. *Curr. Appl. Phys.* **16**, 63–67 (2016).